TASK QUARTERLY 18 No 2, 117–135

SIMULATIONS OF THE PROPERTIES OF ELONGATED HEXAGONAL DODECAHEDRON SYSTEMS

JOSEPH N. GRIMA[1,2], ROBERTO CARUANA-GAUCI[1], DAPHNE ATTARD[1] AND RUBEN GATT[1]

[1]*Metamaterials Unit, Faculty of Science, University of Malta, Msida MSD 2080, Malta*

[2]*Department of Chemistry, Faculty of Science, University of Malta, Msida MSD 2080, Malta*

(Received 20 February 2014; revised manuscript received 25 March 2014)

Abstract: This study considers a 3D basic unit-cell proposed for auxetic and non-auxetic foams namely the elongated hexagonal dodecahedron deforming through changes in angle between its ligaments (idealised hinging model). This structure was studied in detail for the potential of exhibiting negative Poisson's ratio and/or negative compressibility by means of a method based on standard force-field molecular modelling technique, termed as Empirical Modelling Using Dummy Atoms (EMUDA). The mechanical properties obtained from this method were then compared to a previously published analytical model of this structure [Grima J N, Caruana-Gauci R, Attard D, and Gatt R 2012, *Proc. Roy. Soc. A* **468** 3121], and found to be in good agreement with each other. The results showed that this system can exhibit zero Poisson's ratios in one of its planes and positive or negative Poisson's ratios in other planes, depending on the geometry of the model. It was also shown that under certain conditions, negative linear and/or area compressibility was also exhibited.

Keywords: Auxetic; empirical model; negative Poisson's ratio; negative compressibility; cellular structure; foams

1. Introduction

The scope of this paper is to examine in detail the elongated hexagonal dodecahedron 3D structure which is known to be capable of exhibiting positive Poisson's ratio in its non re-entrant form and negative Poisson's ratio in its re-entrant form (Figure 1) [1]. One of the methods which can be employed to examine such a structure is a molecular modelling based technique, where the properties of the structure are simulated. In order to perform such simulations, one requires

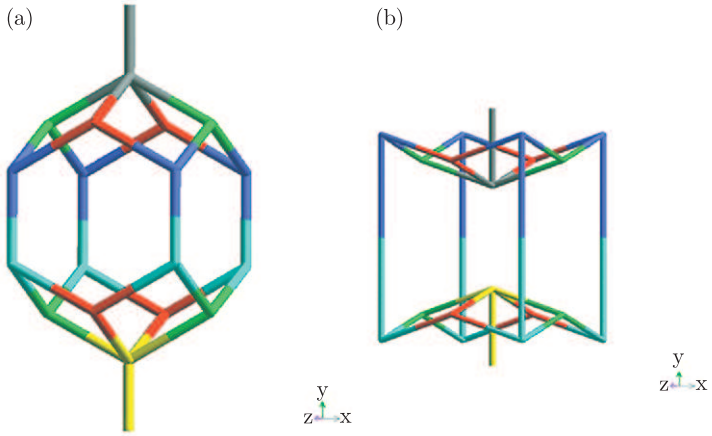

Figure 1. (a) The hexagonal dodecahedron in its non re-entrant form and (b) the elongated hexagonal dodecahedron in its re-entrant form, visualisation rendered by *Cerius*^{2}

a specific molecular modelling software package, such as *Cerius*^{2} which is the molecular modelling package used throughout this paper.

In particular, this paper will make use of the EMUDA technique whenever simulations are performed. The term EMUDA was coined by Grima in 2000 and stands for Empirical Modelling Using Dummy Atoms. This technique was first proposed by Grima [2] and was further developed by Chircop Bray and Grima [3–5] who used it in the analyses and modelling of various auxetic and non-auxetic structures [6–15]. This modelling technique has been well validated and shown to be highly robust and suitable for simulating the mechanical and thermal properties of structures made from ribs which deform through hinging and/or stretching of the ribs. It was also shown that it can be used as a means of comparison and checking with proposed analytical models [3–5].

The EMUDA modelling technique involves the construction of structures made up of dummy atoms, that is, atoms having a nominal mass. In the EMUDA simulations, non-bonding interactions such as Van der Waal's forces are not included. Such non-bonding interactions are usually considered by 'normal' molecular modelling methods, and as a result, the EMUDA technique may be considered as a simplification over such modelling techniques. Another important simplification employed by the EMUDA technique is that the only terms in the energy expression defined in this technique are those specified by the force-field and these are typically the bond lengths between the dummy atoms, the angles in between such atoms and their torsion angles. However, the user may vary the terms which are defined according to his/her intent. This simplistic approach results in the creation of a structure where its ribs consist of 'springs' and where its subtended angles between the bonds consist of 'hinges'.

By the EMUDA technique, one can render a visualisation of a complex structure in such detail that any flaw in the geometry is easily observed and measured. This visualisation of the structure serves as an essential aid for the

user to fully define and understand a structure, something which may not be easy if the structure is three dimensional such as the one being modelled here. In this respect, it should be recalled that one of the biggest advantages brought about by the introduction of molecular modelling is the easy rendering of three dimensional molecules, something which up to a few decades ago could only be done through a laborious process by highly specialised technicians. Also by means of the EMUDA technique, the user can obtain simulated numerical values of mechanical properties such as the Young's modulus of the system, the Poisson's ratio and the compressibility which can then be compared to those obtained by an analytical model or to experimental data, if available.

This paper makes use of the EMUDA technique to construct and simulate a 3D model of an elongated hexagonal dodecahedron with the scope of obtaining a better understanding of its three-dimensional geometry and the properties it may exhibit. In particular, its ability to exhibit negative Poisson's ratio, and possibly other anomalous properties will be examined.

2. Construction of the elongated hexagonal dodecahedron in *Cerius*^{2}

Simulations were performed on a *Cerius*^{2} Version 4.10 (distributed by Accelyrs Inc.) molecular package using a *Silicon Graphics, Inc.* (SGI) Octane2.

The hexagonal dodecahedron structure is made up of ribs having different lengths where the ribs of length l_3 are aligned parallel to the Ox_3 direction whilst the ribs of length l_1 are placed parallel to the Ox_1-Ox_3 plane and the ribs of length l_2 are parallel to the Ox_2-Ox_3 plane.

The simplest non re-entrant hexagonal structure with parameters $l_1 = l_2 = l_3 = 0.1\,\text{nm}$ and $\theta_1 = \theta_2 = 30^\circ$ was first considered. The position of each vertex was calculated, and a dummy atom was placed at each vertex by inputting the calculated co-ordinates (x,y,z) for each atom. The atoms were placed in such a way that the Ox_3 direction of the model is parallel to the z-direction whilst the Ox_2 axis is aligned in the xy-plane of the molecular modelling programme and the Ox_1 is free to take any orientation. However, since the hexagonal dodecahedron structure has got a cubic unit cell, then by default the Ox_1 is parallel to the x-axis, the Ox_2 is parallel to the y-axis whilst the Ox_3 is parallel to the z-axis. The placed atoms were then connected to each other by means of a single bond using the graphic interface of *Cerius*^{2}.

Since the parameters l_1, l_2, l_3, θ_1 and θ_2 are known, the cell parameters of the unit cell in the Ox_1, Ox_2 and Ox_3 directions were calculated by using the respective equations:

$$X_1 = 2l_1\cos(\theta_1) \tag{1}$$

$$X_2 = 2l_2\cos(\theta_2) \tag{2}$$

$$X_3 = 2\left[l_3 + l_1\sin(\theta_1) + l_2\sin(\theta_2)\right] \tag{3}$$

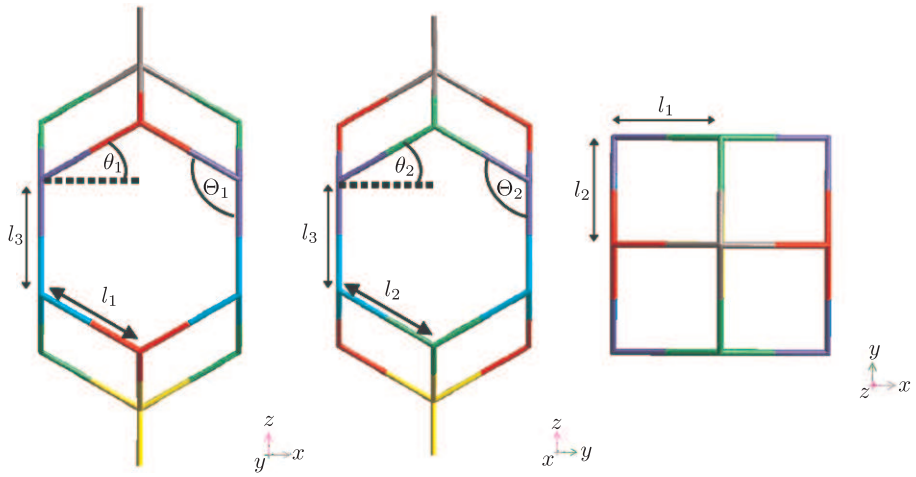

Figure 2. 2D projections of the simplest non re-entrant hexagonal dodecahedron being considered

On obtaining the cell parameters of the unit cell, a boundary condition was then applied so as to produce a 3D tessellation representing an infinite system. After the application of the boundary condition, the structure was checked again and any missing or extra bonds, which typically result from the tessellation process, were added or removed accordingly. This structure was now complete and from now onwards is referred to as the parent structure.

3. Setting up of the energy expression

The 3D elongated hexagonal dodecahedron studied in this work will be one which deforms solely through a mechanism which involves changes in the angles in between the ribs (idealised hinging model). It is important to note that the way how this angle is defined by *Cerius*^{2} is different from the way θ is defined in the model proposed by Evans [1]. In fact, in *Cerius*^{2} the angle Θ was defined to be the whole subtended angle from the slanting rib to the vertical rib. This angle Θ is related to θ by the equation:

$$\theta = \Theta - 90^\circ \tag{4}$$

The user has virtually total control on the type of deformation mechanism placed on the structure by defining the various stiffness constants of the system. In fact, in order for a system to deform solely through hinging, the hinging force constant is taken to be small whereas the stretching bond constant is taken to be very large so as to eliminate any deformation through stretching. Another constraint that needs to be applied on the system is the torsional term. This is because hinging of the angles can occur out-of-plane resulting in a totally new geometry. To prevent such out-of-plane deformation, a very large torsional term is applied in the xy and the yz plane so as to ensure that any hinging of the angles remains solely in-plane and no shearing occurs.

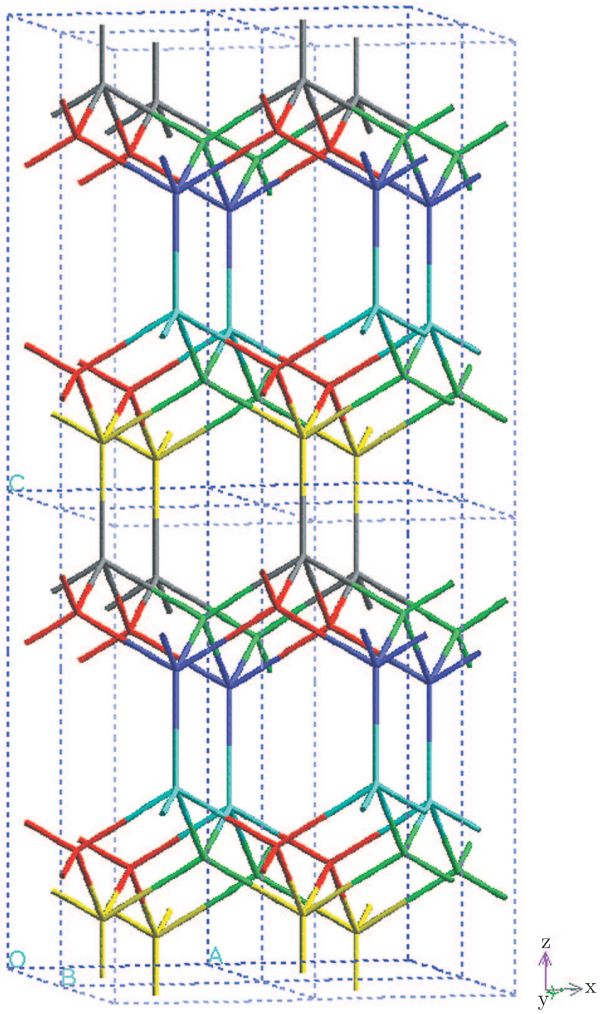

Figure 3. A $(2\times2\times2)$ visualisation of the parent structure

Through the *Cerius*^{2} molecular package, there are several methods how these spring constants could be applied. In this work, the bond stretching and angle bending terms were taken to be harmonic terms whereas the torsional term was taken to be a dihedral cosine term. The bond stretching harmonic potential is given by the equation:

$$V = \frac{1}{2}k_s(l-l_o)^2 \tag{5}$$

where k_s is the stretching force constant, l is the actual bond length and l_o is the target bond length.

The bond angle bending harmonic potential is given by the equation:

$$V = \frac{1}{2}k_h(\theta-\theta_o)^2 \tag{6}$$

where k_h is the hinging force constant, θ is the actual angle bend and θ_o is the target bond bend.

The torsional dihedral cosine term is given by the equation:

$$V = \frac{1}{2} k_t [1 - d\cos(n\phi)] \tag{7}$$

where k_t is the torsion force constant, ϕ is the actual angle between planes, d gives the symmetry present (e.g. *cis*-, *trans*-) and n indicates the number of cycles in 360° rotation of the dihedral. Note that in this work, d was equal to 1 and n is equal to 4 in accordance with the symmetry.

The above terms can be inserted in the system either by means of a force-field or by means of a restraint. In this paper, the force-field method was used. The advantage in using the force-field method lies in the fact that there would be no need to modify the parent structure for every simulation run. Instead, one simply has to generate a force-field which modifies the parent structure when loaded.

For every structure analysed, the potentials, stiffness constants and target lengths and angles were written in a force-field where the only terms being considered are the bond stretch, the angle bend and the bond torsion. All other energy expression terms such as non-bonding terms were considered to be zero. A typical custom-made force field is presented below for a structure with the parameters $l_3 = 1\,\mathrm{nm}$, $l_1 = 0.3\,\mathrm{nm}$, $l_2 = 0.2\,\mathrm{nm}$, $\Theta_1 = 120°$ and $\Theta_2 = 60°$ whilst $k_s = 4.18 \times 10^{-5}\,\mathrm{kJ\,mol^{-1}\,m}$ ($99999.0\,\mathrm{kcal\,mol^{-1}\,Å}$), $k_h = 418.4\,\mathrm{kJ\,mol^{-1}\,rad^{-1}}$ ($100.0\,\mathrm{kcal\,mol^{-1}\,rad^{-1}}$) and $k_t = 4.18 \times 10^{3}\,\mathrm{kJ\,mol^{-1}\,rad^{-1}}$ ($999.0\,\mathrm{kcal\,mol^{-1}\,rad^{-1}}$). Note that the values for k_s and k_t used were the maximum permitted by the molecular package and are much bigger than k_h.

```
001 VERSION
002 CERIUS2 1
003 END
004 #
005 HEADER
006 END
007 #
008 PREFERENCES
009 BONDS T
010 ANGLES T
011 COULOMB F
012 INVERSIONS F
013 TORSIONS T
014 UREY_BRADLEY F
015 HYDROGEN_BONDS F
016 DIAGONAL_VAN_DER_WAALS F
017 OFF_DIAGONAL_VAN_DER_WAALS F
018 GENERATE_UNDEFINED_TERMS F
019 IGNORE_UNDEFINED_TERMS T
020 SHRINK_CH_BONDS F
021 SINGLE_TORSION F
022 SCALE_TORSIONS_ABOUT_COMMON_BOND F
023 EXOCYCLIC_TORSIONS_SCALE_FACTOR 1.00000
024 SINGLE_INVERSION F
```

```
025 H-BOND_METHOD SPLINE
026 H-BOND_LIST F
027 NON_BOND_LIST F
028 DISTANCE_DEPENDENT_DIELETRIC_CONSTANT F
029 COU_DIELETRIC_CONSTANT 1.00000
030 COU_EXCLUDE_1-2 T
031 COU_EXCLUDE_1-3 T
032 COU_EXCLUDE_1-4 F
033 COU_1-4_SCALE_FACTOR 1.00000
034 COU_METHOD SPLINE
035 VDW_RADII_COMBINATION_RULE ARITHMETIC
036 VDW_EXCLUDE_1-2 T
037 VDW_EXCLUDE_1-3 T
038 VDW_EXCLUDE_1-4 F
039 VDW_1-4_SCALE_FACTOR 1.00000
040 VDW_METHOD SPLINE
041 MINIMUM_IMAGE F
042 ASSIGN_MASS T
043 ASSIGN_CHARGE F
044 ASSIGN_HYBRIDIZATION F
045 ATOM_TYPE F
046 ATOM_TYPE_ALL F
047 CALCULATE_BOND_ORDER F
048 END
049 #
050 ATOMTYPES
051 RED C 12.01115
052 CYA C 12.01115
053 WHI C 12.01115
054 GRE C 12.01115
055 YEL C 12.01115
056 BLU C 12.01115
057 END
058 #
060 DIAGONAL_VDW
061 END
062 #
063 ATOM_TYPING_RULES
064 END
065 #
066 #
067 OFF_DIAGONAL_VDW
068 END
069 #
070 BOND_STRETCH
071 CYA BLU HARMONIC 99999.0 10.000
072 YEL WHI HARMONIC 99999.0 10.000
073 BLU RED HARMONIC 99999.0 3.0000
074 GRE YEL HARMONIC 99999.0 3.0000
075 CYA RED HARMONIC 99999.0 3.0000
076 WHI GRE HARMONIC 99999.0 3.0000
077 GRE BLU HARMONIC 99999.0 2.0000
078 YEL RED HARMONIC 99999.0 2.0000
079 WHI RED HARMONIC 99999.0 2.0000
080 CYA GRE HARMONIC 99999.0 2.0000
081 END
082 #
```

```
083 ANGLE_BEND
084 RED BLU CYA THETA_HARM 100.0000 120.000
085 RED CYA BLU THETA_HARM 100.0000 120.000
086 GRE YEL WHI THETA_HARM 100.0000 120.000
087 YEL WHI GRE THETA_HARM 100.0000 120.000
088 GRE CYA BLU THETA_HARM 100.0000 60.0000
089 CYA BLU GRE THETA_HARM 100.0000 60.0000
090 RED YEL WHI THETA_HARM 100.0000 60.0000
091 YEL WHI RED THETA_HARM 100.0000 60.0000
092 END
093 #
094 TORSIONS
095 X BLU CYA X DIHEDRAL 999.0 4.0000 1.0000
096 X YEL WHI X DIHEDRAL 999.0 4.0000 1.0000
097 END
098 #
099 INVERSIONS
100 END
101 #
102 UREY_BRADLEY
103 END
104 #
105 HYDROGEN_BONDS
106 END
107 #
108 GENERATOR
109 END
```

Where:

Lines 001–048 define which terms are included in the energy expression.

Lines 051–056 define the dummy atoms being used for the structure with the syntax;

```
ATOM_TYPE  ELEMENT_TYPE  MASS
```

where; **ATOM_TYPE** is the label of the different atoms being used. In this case, the atoms were labelled as colours in order to pinpoint them on the structure during visualisation. The **ELEMENT_TYPE** was set to be of carbon whereas their **MASS** was considered to be that of carbon, however this is redundant since this does not figure in any calculation.

Lines 071–080 define the bond length between the atoms with the syntax;

```
XX1  XX2  HARMONIC  XX3  XX4
```

where; **XX1** and **XX2** refer to the dummy atoms being bonded together, **HARMONIC** refers to type of potential used *i.e.* the one in equation (5), **XX3** defines the stiffness constant of the bond (since this is taken to be a spring) in $\mathrm{kcal\,mol^{-1}\,\AA}$. The stiffness constant was defined to be the maximum possible so as not to have any stretching in the bond during deformation since the user's intent was to investigate the hinging mechanism. The term **XX4** defines the target bond length in Å. This number varies depending whether it denotes l_3 which is of length 1 nm, l_1 which has a length of 0.3 nm or l_2 which has a length of 0.2 nm.

Lines 084–091 define the bond angles between the atoms with the syntax;

```
XX1  XX2  XX3  THETA_HARM  XX4  XX5
```

where; `XX1`, `XX2` and `XX3` refer to the dummy atoms between which the bond-angle is subtended, `THETA_HARM` refers to the type of potential being used, in this case it is the harmonic potential as defined in equation (6), `XX4` defines the stiffness constant of the bond-angle (since this is taken to be a hinge) in $\mathrm{kcal\,mol^{-1}\,rad^{-1}}$. The stiffness constant was defined to be low when compared to the bond stretching constant so that the system deforms through the hinging mechanism. The term `XX5` defines the target bond angle in degrees. This number varies since Θ_1 was defined to be 120° whereas Θ_2 was defined to be 60°.

Lines 095–096 define the torsion between the atoms with the syntax;

```
XX1  XX2  XX3  XX4  DIHEDRAL  XX5  XX6  XX7
```

where; `XX1`, `XX2`, `XX3` and `XX4` refer to the dummy atoms between which the torsion angles is formed. The term `DIHEDRAL` refers to the type of potential the torsion angle is applied as defined by equation (7). In this paper, the torsional terms were applied around the ribs of length l_3 and thus, `XX2` and `XX3` were given as the pairs `BLU-CYA` and `YEL-WHI` and the values `XX1` and `XX4` were taken to be `X` that is, any atom type in the structure. The term `XX5` defines the stiffness of the torsion angle in $\mathrm{kcal\,mol^{-1}\,\AA}$ which was taken to be the largest possible so that the system does not exhibit shear in the xy plane and the atoms remain in their respective planes. The terms `XX6` and `XX7` define the terms n and d in the dihedral potential equation which were given values of 4 and 1 respectively.

4. Energy expression and mechanical properties calculation

Once the force field was set up correctly, it was then loaded in *Cerius*^{2} molecular package. The structure was then minimised according to the parameters given in the force-field. The minimisation procedure will give the best conformation and the nearest lowest energy profile of the system with the defined parameters.

There are several minimisation algorithms which can be employed to reach the minimum energy profile. Also the user can define the number of iterative steps and the convergence criteria. The minimisation algorithm used for the simulations in this paper was the 'smart minimiser'. This selects the most appropriate minimising algorithm according to the size of the structure and the distance to the minimum. At the beginning, the smart minimiser employs the **Steepest Descent** algorithm. This algorithm is the simplest of the iterative algorithms and functions by changing the direction when a minimum is reached. As a result, it is the most robust of all other algorithms but is much less accurate. Once substantial progress is reached, and since the structure being modelled has less than 100 atoms, the 'smart minimiser' switches to the **Adopted Basis Newton-Raphson** (**ABNR**)

algorithm which is more accurate than the steepest descent algorithm. After more progress, the 'smart minimiser' switches to the **Quasi-Newton-Raphson** which method acts as a bridge between previous less accurate algorithms to more accurate algorithms. Once again, when substantial progress is reached the 'smart minimiser' switches to the **Truncated Newton-Raphson** since the structure has less than 100 atoms. This algorithm is highly accurate and is used to achieve minima with high convergence criteria. However it is computationally and memory intensive and hence it is used as the last type of minimisation.

For these simulations, first, three runs of a maximum of 5000 steps each were run for the structure, or until the *Cerius*^{2} default standard convergence criteria were met, whichever occurs first. The *Cerius*^{2} default convergence criteria state a number of conditions which must be satisfied which include a RMS (Root Mean Square) derivative less than $4.18\times10^{-12}\,\mathrm{kJ\,mol^{-1}m}$ ($0.01\,\mathrm{kcal\,mol^{-1}\AA}$), a maximum overall energy difference of $4.18\times10^{-3}\,\mathrm{kJ\,mol^{-1}}$ ($1\times10^{-3}\,\mathrm{kcal\,mol^{-1}}$) and a maximum RMS stress of 0.1 GPa. These minimisations were then followed by three more minimisations of a maximum of 5000 steps each or until the *Cerius*^{2} high standard criteria were met, whichever occurs first. The high standard convergence criteria state a number of more rigorous conditions which must be satisfied which include a RMS derivative less than $4.18\times10^{-13}\,\mathrm{kJ\,mol^{-1}m}$ ($0.001\,\mathrm{kcal\,mol^{-1}\AA}$), a maximum overall energy difference of $4.18\times10^{-4}\,\mathrm{kJ\,mol^{-1}}$ ($1\times10^{-4}\,\mathrm{kcal\,mol^{-1}}$) and a maximum RMS stress of 1×10^{-3} GPa.

When the nearest minimum energy profile of the system was achieved, the mechanical properties of the system were calculated. The molecular package *Cerius*^{2} allows the calculation of mechanical properties through various methods, however the method employed in this paper is the **second derivative** method. This method gives the second derivatives of the lattice energy with respect to the atomic co-ordinates and the lattice parameters by using a single-point energy calculation. In fact, if one excludes the internal degrees of freedom, which could have been used to simulate the equivalent of the IR spectrum, then one may write:

$$U = U_o + \sum_i \frac{\partial U}{\partial \varepsilon_i}\varepsilon_i + \sum_{i,j} \frac{\partial^2 U}{\partial \varepsilon_i \partial \varepsilon_j}\varepsilon_i\varepsilon_i + \text{higher order terms} \tag{8}$$

where; ε is the strain and U_o is the equilibrium energy. Note that according to this expression, if the first derivatives are zero (*i.e.* the system is at a minimum), then the second derivatives may be easily evaluated if the value of U_o is known and the higher order terms are ignored. The second derivative is then used to calculate the 6×6 components of the stiffness matrix $\mathbf{C}$ (and hence the compliance matrix $\mathbf{S}=\mathbf{C}^{-1}$) since:

$$c_{ij} = \frac{\partial^2 U}{\partial \varepsilon_i \partial \varepsilon_j} \tag{9}$$

The results generated by *Cerius*^{2} are given in two 6×6 matrices where one of them is the stiffness matrix $\mathbf{C}$ whereas the second matrix, the compliance matrix $\mathbf{S}$, is the inverse of the stiffness matrix. Data was extracted from the

obtained compliance matrix by expressing the Young's moduli and the Poisson's ratio follows in terms of s_{ij} as follows:

$$\begin{array}{lll} E_1 = \frac{1}{s_{11}} & E_2 = \frac{1}{s_{22}} & E_3 = \frac{1}{s_{33}} \\ \nu_{12} = -\frac{s_{21}}{s_{11}} & \nu_{23} = -\frac{s_{32}}{s_{22}} & \nu_{31} = -\frac{s_{13}}{s_{33}} \\ \nu_{13} = -\frac{s_{31}}{s_{11}} & \nu_{21} = -\frac{s_{12}}{s_{22}} & \nu_{32} = -\frac{s_{23}}{s_{33}} \end{array} \tag{10}$$

whilst the compressibilities can be calculated by the equations;

$$\begin{array}{lll} \beta_1 = s_{11} + s_{12} + s_{13} & \beta_2 = s_{21} + s_{22} + s_{23} & \beta_3 = s_{31} + s_{32} + s_{33} \\ \beta_{12} = \beta_1 + \beta_2 & \beta_{13} = \beta_1 + \beta_3 & \beta_{23} = \beta_2 + \beta_3 \\ & \beta_{123} = \beta_1 + \beta_2 + \beta_3 & \end{array} \tag{11}$$

Note that the compressibilities may be obtained in terms of the Young's moduli and the Poisson's ratio.

In addition to these simulations, additional simulations were performed by applying a uniaxial stress which is equivalent to 10 % of the Young's moduli or a hydrostatic compressive pressure which is equivalent to 10 % of the bulk modulus so as to visualise the deformations.

5. Results and Discussion

The mechanical properties as simulated by the second derivative method are summarised in (Tables 1 to 3). Images of the deformed structures following the application of uniaxial loads and hydrostatic pressure are shown in (Figure 4 to Figure 6) where the pink box and blue box show the original cell parameters before deformation and after deformation respectively.

The first thing that was noted from the results obtained was that all the simulations were run to completion and that the systems minimised with the correct lengths and angles as stipulated in the force-fields. Furthermore, from the systems minimised at non-zero mechanical loads, there were no changes in the lengths and torsion angles with all the deformations being at the hinging angles, as expected. This is very important as it confirms that the force-fields used were successfully written and loaded and that a nearest minimum energy expression can be achieved in order to calculate the mechanical properties of the system.

The results also show that in the planes where the re-entrant geometry is present, a negative Poisson's ratio was observed upon hinging, whilst in the planes where the geometry is non re-entrant, a positive Poisson's ratio is observed on hinging. These observations can be explained by considering that the structure, on applying a tensile stress, is deforming through a typical honeycomb manner. That is, for example, a tensile stress in the x-direction results in a rotation of the ligament of length l_1 as clearly shown in (Figure 4).

Of particular interest is the fact that from the results obtained, it can be shown that the non re-entrant structure being studied exhibits negative compressibility. This conclusion is not only supported by the numbers obtained (β_3 and β_{13} for the first structure studied) from the mechanical properties but is also

Table 1. Mechanical properties obtained for a system where $l_3 = 1\,\text{nm}$, $l_1 = 0.2\,\text{nm}$, $l_2 = 0.4\,\text{nm}$, $\theta_1 = 105^\circ$ and $\theta_2 = 135^\circ$

E_1 [GPa]	E_2 [GPa]	E_3 [GPa]	ν_{12}	ν_{21}	ν_{13}	ν_{31}	ν_{23}	ν_{32}	β_1 [GPa^{-1}]	β_2 [GPa^{-1}]	β_3 [GPa^{-1}]	β_{12} [GPa^{-1}]	β_{13} [GPa^{-1}]	β_{23} [GPa^{-1}]	β_{123} [GPa^{-1}]
132.24	9.53	144.59	0	0	0.54	0.59	0.21	3.22	3.49×10^{-3}	8.72×10^{-2}	-1.94×10^{-2}	8.62×10^{-2}	-1.59×10^{-2}	6.33×10^{-2}	6.68×10^{-2}

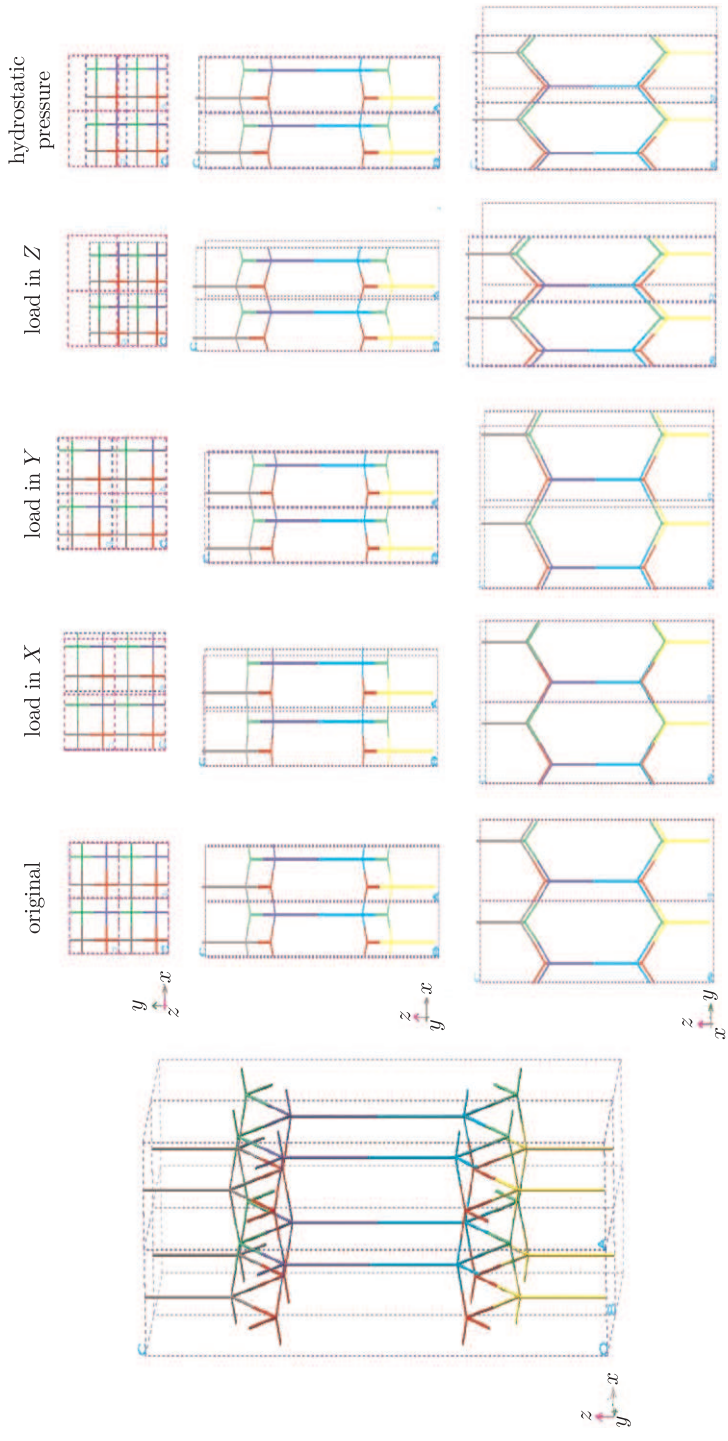

Figure 4. Deformation of a structure system where $l_3 = 1\,\text{nm}$, $l_1 = 0.2\,\text{nm}$, $l_2 = 0.4\,\text{nm}$, $\theta_1 = 105^\circ$ and $\theta_2 = 135^\circ$

Table 2. Mechanical properties obtained for a system where $l_3 = 1\,\text{nm}$, $l_1 = 0.3\,\text{nm}$, $l_2 = 0.2\,\text{nm}$, $\theta_1 = 75°$ and $\theta_2 = 60°$

E_1 [GPa]	E_2 [GPa]	E_3 [GPa]	ν_{12}	ν_{21}	ν_{13}	ν_{31}	ν_{23}	ν_{32}	β_1 [GPa^{-1}]	β_2 [GPa^{-1}]	β_3 [GPa^{-1}]	β_{12} [GPa^{-1}]	β_{13} [GPa^{-1}]	β_{23} [GPa^{-1}]	β_{123} [GPa^{-1}]
234.09	50.46	99.84	0	0	−1.31	−0.56	−0.36	−0.72	9.88×10^{-3}	2.70×10^{-2}	2.28×10^{-2}	3.69×10^{-2}	3.27×10^{-2}	4.99×10^{-2}	5.98×10^{-2}

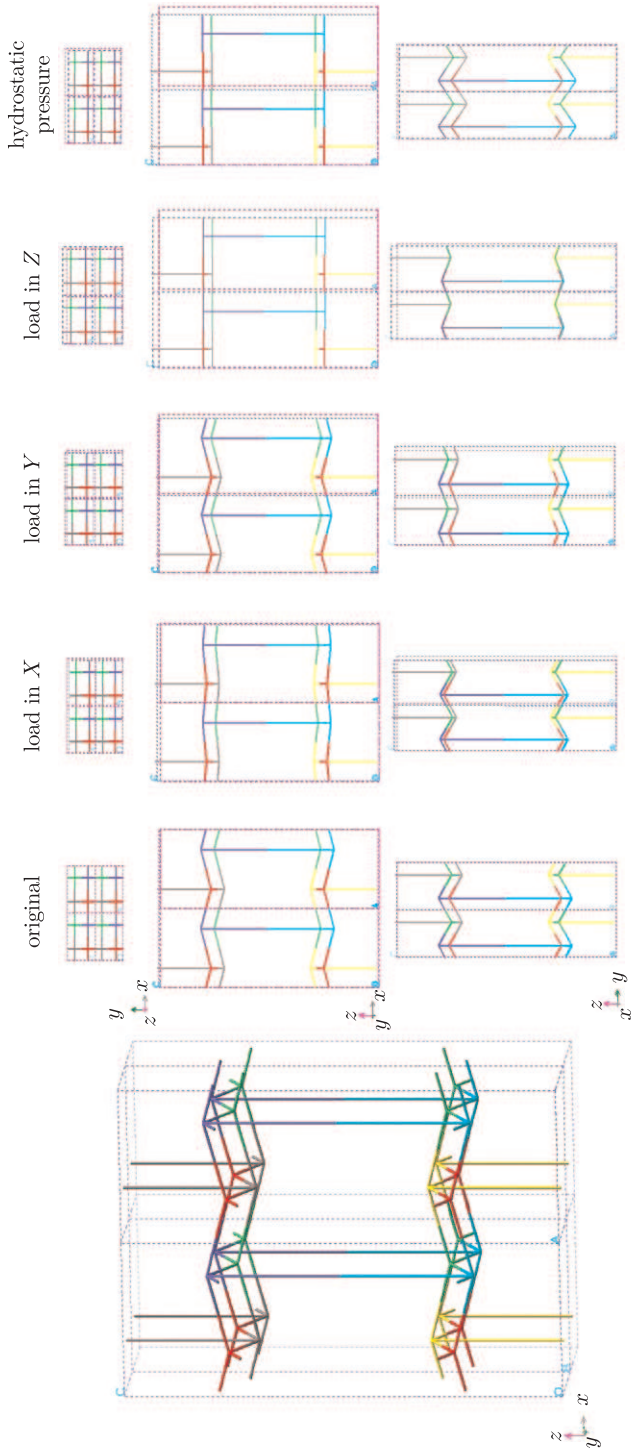

Figure 5. Deformation of a structure system where $l_3 = 1\,\text{nm}$, $l_1 = 0.3\,\text{nm}$, $l_2 = 0.2\,\text{nm}$, $\theta_1 = 75°$ and $\theta_2 = 60°$

Table 3. Mechanical properties obtained for a system where $l_3 = 1\,\text{nm}$, $l_1 = 0.2\,\text{nm}$, $l_2 = 0.3\,\text{nm}$, $\theta_1 = 75°$ and $\theta_2 = 105°$

E_1 [GPa]	E_2 [GPa]	E_3 [GPa]	ν_{12}	ν_{21}	ν_{13}	ν_{31}	ν_{23}	ν_{32}	β_1 [GPa^{-1}]	β_2 [GPa^{-1}]	β_3 [GPa^{-1}]	β_{12} [GPa^{-1}]	β_{13} [GPa^{-1}]	β_{23} [GPa^{-1}]	β_{123} [GPa^{-1}]
167.92	168.24	104.94	0	0	−0.70	−0.44	1.05	0.66	1.01×10^{-2}	-3.12×10^{-4}	7.44×10^{-3}	9.81×10^{-3}	1.76×10^{-2}	7.13×10^{-3}	1.73×10^{-2}

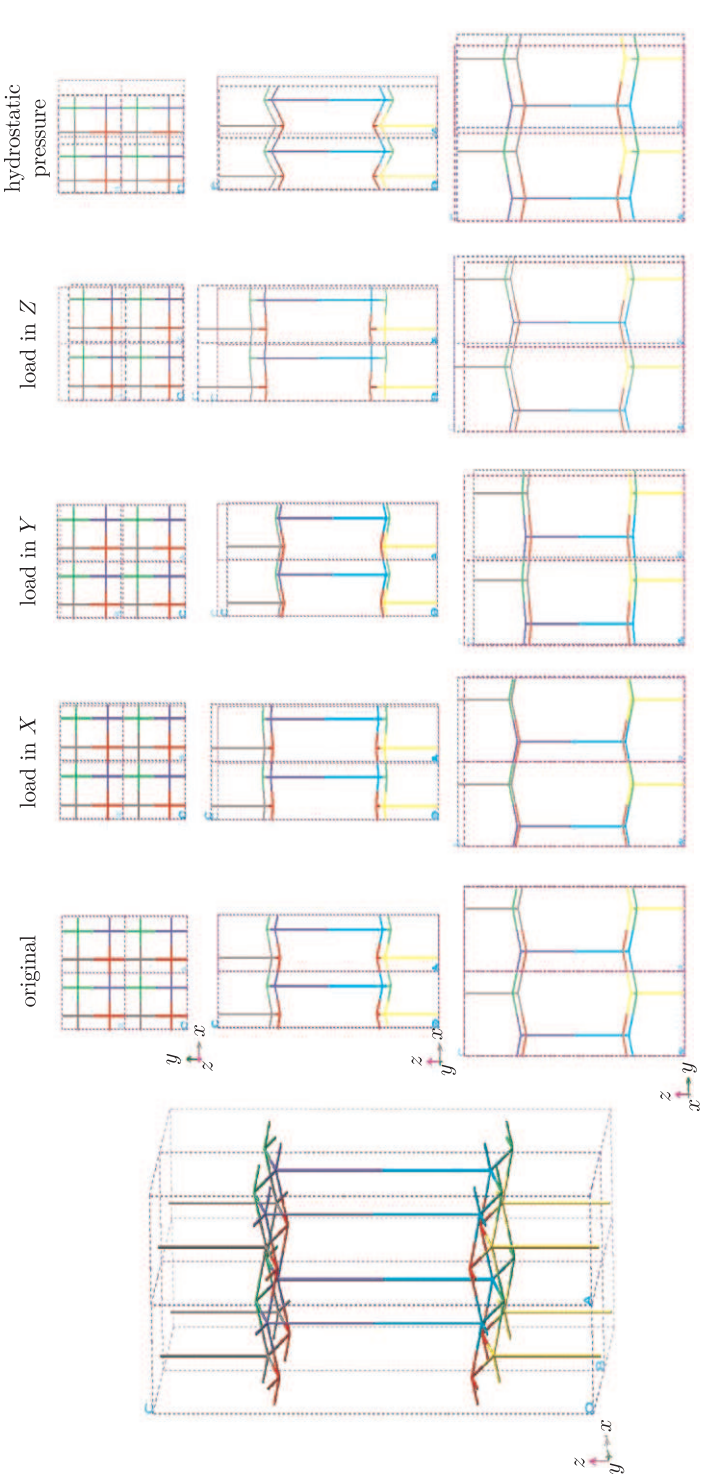

Figure 6. Deformation of a structure system where $l_3 = 1\,\text{nm}$, $l_1 = 0.2\,\text{nm}$, $l_2 = 0.3\,\text{nm}$, $\theta_1 = 75°$ and $\theta_2 = 105°$

supported by the images obtained during deformation. In the deformation images obtained for the first structure (Figure 4), it is clear that when a compressive stress is applied, one of the unit cell sides increases in length. The result obtained is of utmost importance since as previously mentioned, the property of negative compressibility is very rarely exhibited.

Another interesting result is the fact that zero Poisson's ratio is exhibited in the y-direction when loading in the Ox_1 direction, and in the x-direction when loading in the Ox_2 direction. This again is featured both from the results obtained by the mechanical properties and from the deformation images. This occurs since when one applies a tensile stress in the Ox_1 direction, the ribs l_2 which are found in another plane are not affected (and the same applies when applying a tensile stress in the Ox_2 direction, the ribs l_1 are not affected).

6. EMUDA simulations as a validation of the published analytical model

In order to rigorously test the published analytical model of this structure [16] several hundred force-fields were generated by means of a computer script loop. This was done since this is a laborious and a repetitive task, *i.e.* one which makes it ideal to exploit computer resources rather than input the data manually, something which is much more error prone. Since each force-field had different values for every parameter which defines the structure, five script loops had to be written, each loop for every parameter. The first parameter was l_3 and this was defined to take values of 0.8 and 1 nm. When l_3 was defined to be 0.8 nm, l_1 was taken to be 0.2, 0.3 or 0.4 nm (the same applies when $l_3 = 1$ nm). With the second loop defined, a third loop was inserted for the parameter l_2 and this was taken to be either 0.2, 0.3 or 0.4 nm when all the previous parameters take all their possible values. As a result, structures with all three different values of l were possible. Another script loop was written so as to define the value of θ_1 which was given the values $-60°$ to $+150°$ in increments of $15°$ (Note that as previously mentioned, in the force-field the angle Θ is written and this is equal to $\theta + 90°$). The fifth and last loop was written so as to allow θ_2 to take the values of $-60°$ to $+150°$ for every previous θ_1. As a result, apart from having a structure with all three different lengths, the structure could take two different θs simultaneously. Hence in one plane the structure could have the re-entrant geometry whereas in the other plane the structure would have the non re-entrant geometry. In total the amount of structures simulated was of 1458 structures (Number of values of parameters permitted: $l_3 \times l_1 \times l_2 \times \theta_1 \times \theta_2 = 2 \times 3 \times 3 \times 9 \times 9$).

During these simulations, it was assumed that the diameter of the ribs is negligibly small when compared to the other dimensions. Also the torsion energy term was applied in such a manner so as not to permit shearing of the structure. An important restriction which was applied on the structure was that the ribs cannot overlap each other; this was done so as to achieve a physically realisable structure. Due to this last restraint, some combinations of lengths and angles

were not permitted. In fact, it may be shown that the following conditions must be satisfied to permit realisable structures:

$$l_3 > 2l_1 \sin(\theta_1) \tag{12}$$

$$l_3 = 2l_2 \sin(\theta_2) \tag{13}$$

$$l_3 = 2l_1 \sin(\theta_1) + 2l_2 \sin(\theta_2) \tag{14}$$

Note that for the structure to be physically realisable, all the above conditions need to be fulfilled simultaneously, if one of the above conditions is not obeyed, then the structure is not physically realisable.

Once the data was generated, another computer script was written so as to extract the stiffness matrix from the respective second derivative result files and write them in just one file which was then used as a comparison for the results obtained by the previoulsy published analytical model [16]. Direct comparison of the EMUDA results with the analytical model is not possible before some conversions are taken into consideration. This is because the *Cerius*^{2} molecular package uses some non SI units by default (as is normally the case in molecular modelling simulations) whereas the units in the analytical model were SI units. Table 4 summarises the conversion factors that need to be taken.

Table 4. Conversion factors that need to be applied to compare the EMUDA results with the analytical model

Parameter in analytical equation	Parameter in the EMUDA model	Conversion factor	Calculated as
h [m]	h [Å]	$\times 10^{-10}$	Å $\rightarrow$ m: 10^{-10}
l [m]	l [Å]	$\times 10^{-10}$	Å $\rightarrow$ m: 10^{-10}
K_h [J rad^{-2}]	K_h [kcal mol^{-1} rad^{-2}]	$\times 4184 N_A$	kcal $\rightarrow$ J: 4.184×10^3 moles $\rightarrow$ units: N_A
K_s [J m^{-2}]	K_s [kcal mol^{-1} Å^{-2}]	$\times 4184 N_A \times 10^{20}$	kcal $\rightarrow$ J: 4.184×10^3 moles $\rightarrow$ units: N_A Å^{-2} $\rightarrow$ m^{-2}: $(10^{-10})^{-2}$

Plots which compare the results obtained by the EMUDA simulations with those predicted by the analytical model of [16] are shown in Figure 7 and Figure 8.

These results clearly show that, in general, there is excellent agreement between the results of the detailed simulations and the predictions made by the analytical model [16]. This is very important since it gives added confidence to the quality of the results obtained by the two independent methodologies.

7. Conclusion

This paper has presented a modelling methodology and the results obtained for simulating the elongated hexagonal dodecahedron structure. It has been shown that:

- The simulations carried out by the EMUDA technique are working correctly and the mechanical properties of the system can be obtained from the simulation.

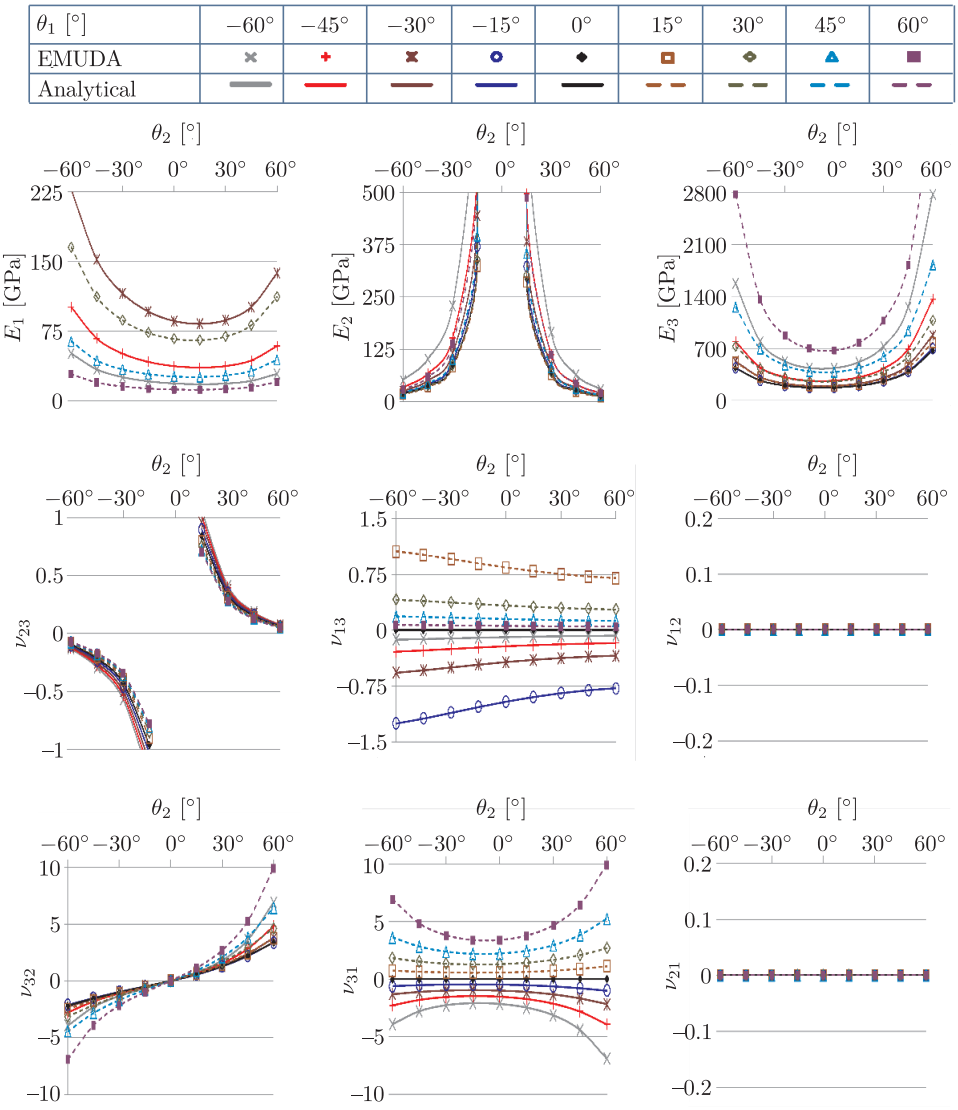

Figure 7. Plots comparing the results for the Young's moduli and the Poisson's ratios obtained from the analytical model [16] and the EMUDA simulations for a system with $l_3 = 0.8\,\text{nm}$, $l_1 = 0.2\,\text{nm}$ and $l_2 = 0.2\,\text{nm}$

- The elongated hexagonal dodecahedron structure exhibits negative or positive Poisson's ratio depending on the type of geometry present resulting in a potential system which has zero/positive/negative Poisson's ratios in three different planes.
- The studied structure can exhibit the rare property of negative compressibility.
- The results obtained from the EMUDA simulations are in agreement with the analytical model [16].

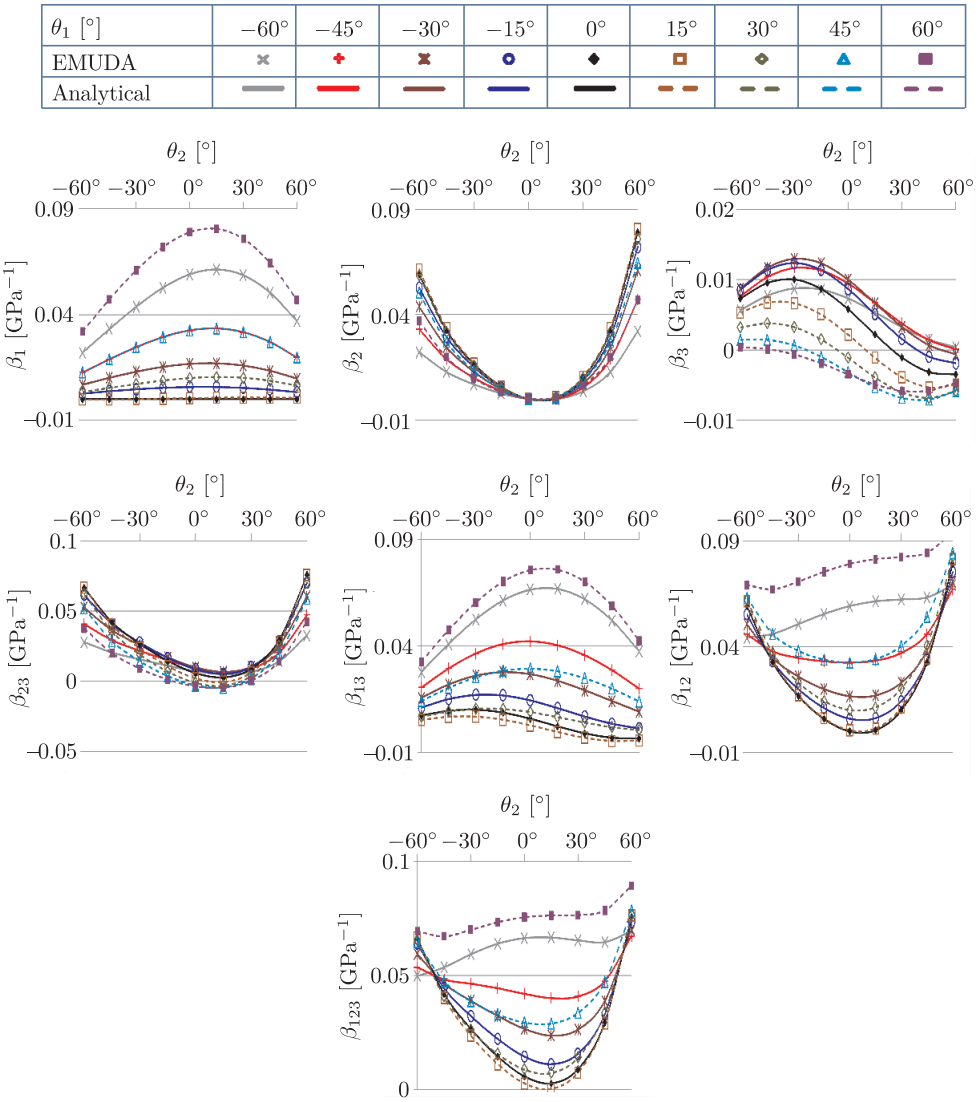

Figure 8. Plots comparing the results for linear, area and volume compressibility obtained from the analytical model [16] and the EMUDA simulations for a system with $l_3 = 0.8\,\text{nm}$, $l_1 = 0.2\,\text{nm}$ and $l_2 = 0.2\,\text{nm}$

References

[1] Evans K E, Nkansah M A and Hutchinson I J 1994 *Acta Metall. Mater.* **42** 1289

[2] Grima J N 2000 *New Auxetic Materials*, PhD Dissertation, University of Exeter, UK

[3] Chircop Bray T G 2005 *Empirical Modelling of 'Negative Structures' using molecular modelling techniques*, B. Sc. (Hons.) Dissertation, University of Malta, Malta

[4] Grima J N, Gatt R, Chircop Bray T G, Alderson A, and Evans K E 2005 *Molecular Simulation* **31** 915

[5] Chircop Bray T G 2007 *EMUDA modelling of 2D and 3D auxetic systems*, M. Sc. Dissertation, University of Malta, Malta

[6] Lakes R S 1987 *Science* **235** 10838
[7] Wojciechowski K W and Branka A C 1989 *Physical Review A* **40** 7222
[8] Evans K E, Nkansah M A, Hutchinson I J and Rogers S C 1991 *Nature* **253** 124
[9] Milton G W 1992 *J. Mech. Phys. Sol.* **40** 1105
[10] Yeganeh-Haeri A, Weidner D J and Parise J B 1992 *Science* **257** 650
[11] He C, Liu P and Griffin A C 1998 *Macromolecules* **31** 3145
[12] Alderson A 1999 *Chem. Ind.* 384
[13] Evans K E and Alderson A 2000 *Adv. Mater.* **12** 617
[14] Scarpa F and Tomlin P J 2000 *Fatigue Fract. Eng. Mater.* **23** 717
[15] Baughman R H 2003 *Nature* **425** 667
[16] Grima J N, Caruana-Gauci R, Attard D, and Gatt R 2012 *Proc. Roy. Soc. A* **468** 3121